Field Orientation Based on Current Amplitude and Phase Angle Control for Wireless Power Transfer

Qi Zhu, *Graduate Student Member, IEEE*, Mei Su, Yao Sun, *Member, IEEE*, Weiyi Tang, and Aiguo Patrick Hu, *Senior Member, IEEE*

***Abstract*—The low coupling coefficient between the transmitter and receiver is the major constraint of a wireless power transfer (WPT) system. Although some approaches, such as increasing the quality factor and achieving precise impedance matching, can reduce the adverse impacts of the low coupling coefficient and improve the system performance, high leakage magnetic flux between the transmitter and receiver remains a problem. With the increase in transfer distance and the misalignment between the transmitter and receiver, the increasing leakage magnetic flux of nondirectional fields degrades the WPT system performance. This paper proposes an active field orientation method to shape the magnetic flux so as to minimize the leakage flux. The amplitude and phase angle of the magnetizing current are controlled, and a coil structure for minimizing the coupling among the transmitters and generating a three-dimensional magnetic field is proposed. This method realizes three-dimension full-range field orientation with adjustable magnitude and direction of B-field at an arbitrary point, and as a result the B-field is concentrated with reduced leakage magnetic flux. The proposed field orientation shaping technique is verified by theoretical analysis, simulation, and experimental results.**

***Index Terms*—Current amplitude and phase angle control, field orientation shaping, leakage magnetic field, wireless power transfer (WPT).**

I. Introduction

WIRELESS power transfer (WPT) has attracted much attention due to the convenience, simplicity, and safety. But when it is used for home appliances, implementable biomedical devices, and electric vehicles, the demand for a large transfer distance and efficiency still needs to be satisfied. Hence, the main issues the recent studies are focusing on include the tradeoff between transfer efficiency and distance, and the spatial freedom between the transmitter and receiver. In order to increase the transfer distance, several studies introduced magnetic resonant coupling to realize the transmission distance beyond the range of near field [1]–[5]. Based on the previous studies, the transfer distance has been increased by adding repeaters between the transmission and receiver coils [6], [7]. To improve the energy transfer efficiency, devices along with new antenna materials and structure have been exploited, such as power amplifiers and dc–dc converters [8]. Meanwhile, if the spatial freedom of WPT has been improved, the electric equipment powered by WPT will have higher mobility. Adjustable impedance matching and multiple transmitter resonant coil topologies have been introduced to expand the spatial freedom of the WPT system [9–12]. However, even with state-of-the-art technologies, improvements in transfer efficiency and distance, and spatial freedom have become saturated. Optimizing the control of the shape of magnetic field, as a new technique further advancing WPT, has attracted more attention [13]. Magnetic field shaping technology has been regarded as a new approach in WPT systems with the feature of the shaped magnetic field pointing to a specific direction, hence, increasing the transfer efficiency and reducing unnecessary flux leakage. Magnetic field shaping technology includes passive and active methods. In the passive methods, a magnetic core is used to provide a path with low magnetic resistance for magnetic flux, which further strengthens the magnetic flux linkage between the transmitter side and the receiver side [14]. In the active method, the magnetic field is shaped by changing the distribution of current flowing in the antenna [13], [15]. In order to satisfy both the demands of distance and spatial freedom, Lim and Park [15] have proposed a novel WPT system based on an active magnetic field shaping technique with two crossed-loop coils. The shaped magnetic field forms an energy beam directing to the receiver coil so that less leakage magnetic flux will exist in the space, the transfer distance can be further extended as compared with the conventional method. The current phase control method shapes the magnetic field in the range of two coils and the orientation of magnetic field can be controlled

Manuscript received March 2, 2017; revised June 2, 2017 and July 18, 2017; accepted October 13, 2017. Date of publication October 30, 2017; date of current version February 13, 2018. This work was supported in part by the National Natural Science Foundation of China under Grant 51677195 and Grant 61622311 and in part by the scholarship from the China Scholarship Council under Grant CSC 201706370068. *(Corresponding author: Yao Sun.)*

Q. Zhu, M. Su, Y. Sun, and W. Tang are with the School of Information Science and Engineering, Central South University, Changsha 410083, China (e-mail: csu_zhuqi@163.com; sumeicsu@csu.edu.cn; yaosuncsu@gmail.com; tangweiyi_nb@163.com).

A. P. Hu is with the Department of Electrical and Computer Engineering, University of Auckland, Auckland 1142, New Zealand (e-mail: a.hu@auckland.ac.nz).

Color versions of one or more of the figures in this paper are available online at http://ieeexplore.ieee.org.

Digital Object Identifier 10.1109/TIE.2017.2767556

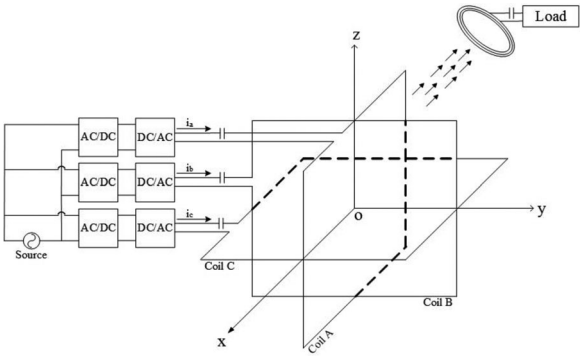

Fig. 1. Block diagram of the proposed WPT system.

to any direction. However, the direction of shaped magnetic field is limited in a two-dimensional (2-D) transection, and the magnetic flux density at a given point in the whole 3-D space is unadjustable.

This paper proposes an active field orientation method to shape the magnetic flux so as to minimize the leakage flux; meanwhile, by controlling the amplitude and phase angle of the magnetizing current, a 3-D magnetic field for WPT with adjustable magnitude and direction is generated. The major study in this paper can be summarized as follows.

1) The detailed synthesis of magnetic field generated by three transmitter coils at an arbitrary point is presented.
2) The 3-D magnetic field orientation is realized by current amplitude and phase angle control.
3) A prototype WPT system for 3-D magnetic field orientation is implementation.

The rest of the paper is organized as follows. In Section II, the coils structure choice and design are explained. In Section III, the distribution and synthesis of B-filed generated by crossed-loop coils are explained. In Section IV, the field orientation based on current amplitude and phase angle control is explained. In Section V, the hardware implementation is introduced, and the experimental results are shown. In Section VI, a conclusion is drawn, and future application of the proposed method is suggested.

II. Coils Structure Design

In order to maximize the magnetic field formed in the near-field range of coils, the WPT coils are often in the shape of a coil or loop. The maximization of coupling between the transmitter and receiver coils and the minimization of leakage flux in the space will improve the efficiency and increase the distance; meanwhile, the minimization of the coupling among the transmitter coils that are used to shape the magnetic field is necessary. This paper introduces a 3-D full-range field orientation technique based on amplitude and phase control of three independent currents. The block diagram of the proposed WPT system is shown in Fig. 1.

This study considers the three crossed-loop transmitter coils structure to keep the coupling among transmitting coils as low as possible and avoid magnetic resonance failure when magnetic coupling occurs among transmitter coils. Fig. 2 shows the detailed structure of the proposed coils.

According to Neumann's formula, we have

$$\begin{aligned} M_{12} &= \frac{\mu_0}{4\pi}\oint\oint\frac{\overline{dl_1}\cdot\overline{dl_2}}{d_{12}} \\ &= \frac{\mu_0}{4\pi}\left(2\int_{-b}^{b}\int_{-a}^{a}\frac{\cos\theta dxdy}{\sqrt{x^2+y^2-2xy\cos\theta}}\right. \\ &\quad -2\int_{-b}^{b}\int_{-a}^{a}\frac{\cos\theta dxdy}{\sqrt{x^2+y^2-2xy\cos\theta+(2c)^2}} \\ &\quad -\int_{-c}^{c}\int_{-c}^{c}\frac{dz\,dz}{\sqrt{(z_1-z_2)^2+d_1^2}}-\int_{-c}^{c}\int_{-c}^{c}\frac{dz\,dz}{\sqrt{(z_3-z_4)^2+d_1^2}} \\ &\quad \left.+\int_{-c}^{c}\int_{-c}^{c}\frac{dz\,dz}{\sqrt{(z_2-z_3)^2+d_2^2}}+\int_{-c}^{c}\int_{-c}^{c}\frac{dz\,dz}{\sqrt{(z_4-z_1)^2+d_2^2}}\right). \end{aligned} \tag{1}$$

So, all the conditions that the coupling of two wires occurs are classified into the following four groups.

1) Two equal-length wires placed in parallel at a distance d: between coils 1 and 2—contours A and E, contours A and G, contours C and E, and contours C and G; between coils 1 and 3—contours B and I, contours B and K, contours D and I, and contours D and K; between coils 2 and 3—contours H and L, contours H and J, contours F and L, and contours F and J. The mutual inductance M_1 can be calculated by the following equation:

$$M_1(l,d) = 0.002\cdot l\cdot\left(\ln\left(\frac{l}{d}+\sqrt{1+\left(\frac{l}{d}\right)^2}\right)-\sqrt{1+\left(\frac{d}{l}\right)^2}+\left(\frac{d}{l}\right)^2\right) \tag{2}$$

where l is the length of the contour, and d is the distance between the two contours.

2) Two wires of unequal lengths are placed with an angle θ on the same plane: between coils 1 and 2—contours B and F, and contours D and H; between coils 1 and 3—contours A and L, and contours C and J; between coils 2 and 3—contours E and I, and contours G and K. The mutual inductance M_2 can be calculated by the following equation:

$$M_2(l_1,l_2,d,\theta) = 0.002\cdot\cos\theta\cdot\left[\frac{l_1}{2}\cdot\tanh^{-1}\left(\frac{\frac{l_2}{2}}{d+\frac{l_1}{2}}\right)+\frac{l_2}{2}\cdot\tanh^{-1}\left(\frac{\frac{l_1}{2}}{d+\frac{l_2}{2}}\right)\right] \tag{3}$$

where l_1 and l_2 are the lengths of the two contours, respectively, d is the distance between the ends of the two contours, and θ is the angle between the two crossed contours.

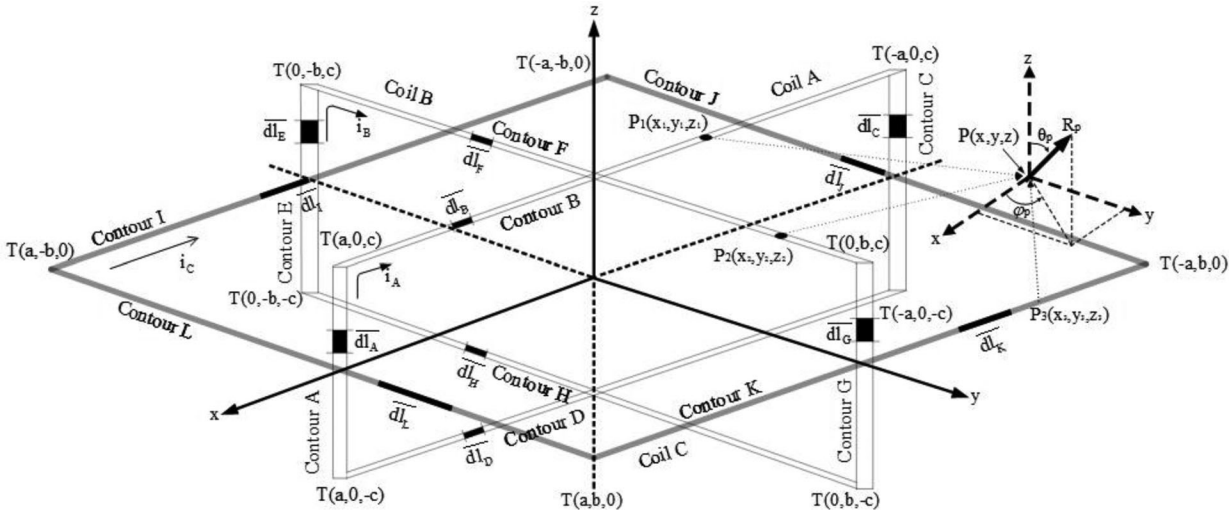

Fig. 2. Detailed structure of the proposed coils.

3) Noncoplanar wires of unequal length were apart from each plane by $2a$ or $2b$ or $2c$: between coils 1 and 2($2c$)—contours B and H, and contours D and F; between coils 1 and 3($2a$)—contours A and J, and contours C and L; between coils 2 and 3($2b$)—contours E and K, and contours G and I. The mutual inductance M_3 can be calculated by the following equation:

$$M_3(l_1,l_2,d,l,\theta) = 0.002\cdot\cos\theta \cdot\left[\frac{l_1}{2}\cdot\tanh^{-1}\left(\frac{\frac{l_2}{2}}{\sqrt{d^2+l^2}+\sqrt{\left(\frac{l_1}{2}\right)^2+l^2}}\right)+\frac{l_2}{2}\cdot\tanh^{-1}\left(\frac{\frac{l_1}{2}}{\sqrt{d^2+l^2}+\sqrt{\left(\frac{l_2}{2}\right)^2+l^2}}\right)-\frac{\Omega(l)}{\sin\theta}\right] \quad (4)$$

$$\Omega(l) = \tan^{-1}\left(\frac{l^2\cos\theta+\frac{l_1 l_2}{4}\sin^2\theta}{l\sqrt{d^2+l^2}\sin\theta}\right) - \tan^{-1}\left(\frac{l\cos\theta}{\sqrt{\left(\frac{l_1}{2}\right)^2+l^2}\sin\theta}\right) - \tan^{-1}\left(\frac{l\cos\theta}{\sqrt{\left(\frac{l_2}{2}\right)^2+l^2}\sin\theta}\right)+\tan^{-1}\left(\frac{\cos\theta}{\sin\theta}\right) \quad (5)$$

where l_1 and l_2 are the lengths of the two contours, respectively, d is the distance between the ends of the two contours projected on the same plane, l is the distance between the two planes, and θ is the angle between the two crossed contours.

4) Two wires are perpendicular to each other, the mutual inductance of two perpendicular wires is zero: between coils 1 and 2—contours A and F, contours A and H, contours C and F, contours C and H, contours B and E, contours B and G, contours D and E, and contours D and G; between coils 1 and 3—contours A and I, contours A and K, contours C and I, contours C and K, contours B and L, contours B and J, contours D and L, and contours D and J; between coils 2 and 3—contours E and L, contours E and J, contours G and L, contours G and J, contours F and I, contours F and I, contours F and K, contours H and I, and contours H and K.

For example, the total mutual inductance M_{12} between coils 1 and 2 can be the summation of M_1, M_2, and M_3 ("+" means the same current direction, "–" means the opposite current direction)

$$\begin{aligned} M_{AE} &= M_{CG} = M_1(2c,d_2),\ M_{AG} \\ &= M_{CE} = -M_1(2c,d_1) \end{aligned} \quad (6)$$

$$\begin{aligned} M_{BF} &= \sum M_2(l_1,l_2,d,\theta) \\ &= M_{B+F+} + M_{B+F-} + M_{B-F-} + M_{B-F+} \\ &= M_2(2a,2b,d_2,\pi-\theta) - M_2(2a,2b,d_1,\theta) \\ &\quad - M_2(2a,2b,d_1,\theta) + M_2(2a,2b,d_2,\pi-\theta) \\ &= 2M_2(2a,2b,d_2,\pi-\theta) - 2M_2(2a,2b,d_1,\theta) \end{aligned} \quad (7)$$

$$\begin{aligned} M_{DH} &= \sum M_2(l_1,l_2,d,\theta) \\ &= M_{D+H+} + M_{D+H-} + M_{D-H-} + M_{D-H+} \\ &= M_2(2a,2b,d_2,\pi-\theta) - M_2(2a,2b,d_1,\theta) \\ &\quad - M_2(2a,2b,d_1,\theta) + M_2(2a,2b,d_2,\pi-\theta) \\ &= 2M_2(2a,2b,d_2,\pi-\theta) - 2M_2(2a,2b,d_1,\theta) \end{aligned} \quad (8)$$

$$\begin{aligned} M_{BH} &= \sum M_3(l_1,l_2,d,l,\theta) \\ &= M_{B+H+} + M_{B+H-} + M_{B-H-} + M_{B-H+} \\ &= -M_3(2a,2b,d_2,2c,\pi-\theta) + M_3(2a,2b,d_1,2c,\theta) \\ &\quad + M_3(2a,2b,d_1,2c,\theta) - M_3(2a,2b,d_2,2c,\pi-\theta) \\ &= 2M_3(2a,2b,d_1,2c,\theta) - 2M_3(2a,2b,d_2,2c,\pi-\theta) \end{aligned} \quad (9)$$

$$\begin{aligned} M_{DF} &= \sum M_3\left(l_1, l_2, d, l, \theta\right) \\ &= M_{D+F+} + M_{D+F-} + M_{D-F-} + M_{D-F+} \\ &= -M_3\left(2a, 2b, d_2, 2c, \pi-\theta\right) + M_3\left(2a, 2b, d_1, 2c, \theta\right) \\ &\quad + M_3\left(2a, 2b, d_1, 2c, \theta\right) - M_3\left(2a, 2b, d_2, 2c, \pi-\theta\right) \\ &= 2M_3\left(2a, 2b, d_1, 2c, \theta\right) - 2M_3\left(2a, 2b, d_2, 2c, \pi-\theta\right). \end{aligned} \tag{10}$$

Hence, according to (6)–(10), M_{12} is expressed as follow:

$$\begin{aligned} M_{12} &= M_{AE} + M_{AG} + M_{CE} + M_{CG} + M_{BF} \\ &\quad + M_{DH} + M_{BH} + M_{DF} \\ &= 2\left[M_1\left(2c, d_2\right) - M_1\left(2c, d_1\right)\right] \\ &\quad + 4\left[M_2\left(2a, 2b, d_2, \pi-\theta\right) - M_2\left(2a, 2b, d_1, \theta\right)\right] \\ &\quad + 4\left[M_3\left(2a, 2b, d_1, 2c, \theta\right) - M_3\left(2a, 2b, d_2, 2c, \pi-\theta\right)\right]. \end{aligned} \tag{11}$$

From (2)–(11), when $d_1 = d_2$ and $\theta = \pi - \theta$, $M_{12} = 0$, the two coils should be perpendicular and have the same length ($a = b$). Based on the same principle, the total mutual inductance M_{13} between coils 1 and 3 and the total mutual inductance M_{23} between coils 2 and 3 can be zero when these three coils are perpendicular and have the same length ($a = b = c$).

The following sections are based on the three orthographically assembled coils structure, which effectively reduces the mutual inductance between the transmitter coils to avoid system performance degradation and is beneficial for the simplification of synthesis of magnetic field. If the structure has slight deformation, the mutual inductance between the transmitter coils increases and the precise impedance matching between the transmitter and receiver becomes a little more difficult, and the three vectors of magnetic field generated by three coils are not orthogonal. However, the synthesis of magnetic field can be still realized by three nonorthogonal B-field vectors, which will be more complex, and the magnetic field orientation can still work if the performance degradation caused by structure deformation is acceptable.

III. Magnetic Flux Density Analysis and Synthesis of Crossed-Loop Coils

According to Fig. 2, coil A lies on the XOZ plane, coil B lies on the YOZ plane, and coil C lies on the XOY plane. The direction of the contours of each coil can be expressed in vector form

$$\begin{aligned} &\overline{dl_A} = \hat{e}_z dz,\ \overline{dl_B} = \hat{e}_x dx,\ \overline{dl_C} = \hat{e}_z dz,\ \overline{dl_D} = \hat{e}_x dx, \\ &\overline{dl_E} = \hat{e}_z dz,\ \overline{dl_F} = \hat{e}_y dy,\ \overline{dl_G} = \hat{e}_z dz,\ \overline{dl_H} = \hat{e}_y dy, \\ &\overline{dl_I} = \hat{e}_x dx,\ \overline{dl_J} = \hat{e}_y dy,\ \overline{dl_K} = \hat{e}_x dx,\ \overline{dl_L} = \hat{e}_y dy. \end{aligned} \tag{12}$$

Assume that a point A on the coil A $p_1(x_1, y_1, z_1)$, a point B on the coil B $p_2(x_2, y_2, z_2)$, a point C on the coil C $p_3(x_3, y_3, z_3)$, and an arbitrary point P $p(x, y, z)$ in the space.

The unit vector $\hat{r}_1$ from A to P, $\hat{r}_2$ from B to P, and $\hat{r}_3$ from C to P are

$$\begin{cases} \hat{r}_1 = \dfrac{\overrightarrow{\mathrm{AP}}}{\left|\overrightarrow{\mathrm{AP}}\right|} = \dfrac{(x-x_1)\hat{e}_x + (y-y_1)\hat{e}_y + (z-z_1)\hat{e}_z}{\sqrt{(x-x_1)^2 + (y-y_1)^2 + (z-z_1)^2}} \\ \hat{r}_2 = \dfrac{\overrightarrow{\mathrm{BP}}}{\left|\overrightarrow{\mathrm{BP}}\right|} = \dfrac{(x-x_2)\hat{e}_x + (y-y_2)\hat{e}_y + (z-z_2)\hat{e}_z}{\sqrt{(x-x_2)^2 + (y-y_2)^2 + (z-z_2)^2}} \\ \hat{r}_3 = \dfrac{\overrightarrow{\mathrm{CP}}}{\left|\overrightarrow{\mathrm{CP}}\right|} = \dfrac{(x-x_3)\hat{e}_x + (y-y_3)\hat{e}_y + (z-z_3)\hat{e}_z}{\sqrt{(x-x_3)^2 + (y-y_3)^2 + (z-z_3)^2}}. \end{cases} \tag{13}$$

Assume that three currents through coils A, B, and C are $I_A\cos(\omega t + \theta_A)$, $I_B\cos(\omega t + \theta_B)$, and $I_C\cos(\omega t + \theta_C)$, respectively. Based on the Biot–Savart law, the magnetic flux density components generated by coils A, B, and C at point P are calculated as follows (the number of turns of each coil is N):

$$\begin{aligned} \overline{B_{\mathrm{Coil}.A}} &= \oint \frac{\mu_0}{4\pi} \frac{NI_A\cos\left(\omega t + \theta_A\right)\overline{dl} \times \hat{r}_1}{r_1^2} \\ &= \frac{\mu_0 NI_A\cos\left(\omega t + \theta_A\right)}{4\pi} \\ &\quad \times \oint \frac{\overline{dl} \times \left[\left(x-x_1\right)\hat{e}_x + \left(y-y_1\right)\hat{e}_y + \left(z-z_1\right)\hat{e}_z\right]}{\left(\left(x-x_1\right)^2 + \left(y-y_1\right)^2 + \left(z-z_1\right)^2\right)^{3/2}} \\ &= \frac{\mu_0 NI_A\cos\left(\omega t + \theta_A\right)}{4\pi} \\ &\quad \times \left\{ \int_A \frac{1}{r_1^3}\left[\hat{e}_y\left(x-x_1\right)dz - \hat{e}_x\left(y-y_1\right)dz\right] \right. \\ &\quad + \int_B \frac{1}{r_1^3}\left[\hat{e}_z\left(y-y_1\right)dx - \hat{e}_y\left(z-z_1\right)dx\right] \\ &\quad + \int_C \frac{1}{{r_1}^3}\left[\hat{e}_y\left(x-x_1\right)dz - \hat{e}_x\left(y-y_1\right)dz\right] \\ &\quad \left. + \int_D \frac{1}{{r_1}^3}\left[\hat{e}_z\left(y-y_1\right)dx - \hat{e}_y\left(z-z_1\right)dx\right] \right\} \\ \overline{B_{\mathrm{Coil}.B}} &= \oint \frac{\mu_0}{4\pi} \frac{NI_B\cos\left(\omega t + \theta_B\right)\overline{dl} \times \hat{r}_2}{r_2^2} \\ &= \frac{\mu_0 NI_B\cos\left(\omega t + \theta_B\right)}{4\pi} \\ &\quad \times \oint \frac{\overline{dl} \times \left[\left(x-x_2\right)\hat{e}_x + \left(y-y_2\right)\hat{e}_y + \left(z-z_2\right)\hat{e}_z\right]}{\left(\left(x-x_1\right)^2 + \left(y-y_1\right)^2 + \left(z-z_1\right)^2\right)^{3/2}} \\ &= \frac{\mu_0 NI_B\cos\left(\omega t + \theta_B\right)}{4\pi} \\ &\quad \times \left\{ \int_E \frac{1}{r_2^3}\left[\hat{e}_y\left(x-x_2\right)dz - \hat{e}_x\left(y-y_2\right)dz\right] \right. \\ &\quad \left. + \int_F \frac{1}{r_2^3}\left[-\hat{e}_z\left(x-x_2\right)dy - \hat{e}_x\left(z-z_2\right)dy\right] \right. \end{aligned} \tag{14}$$

$$+\int_G \frac{1}{{r_2}^3}\left[\hat{e}_y\left(x-x_2\right)dz-\hat{e}_x\left(y-y_2\right)dz\right]$$
$$+\int_H \frac{1}{r_2^3}\left[-\hat{e}_z\left(x-x_2\right)dy+\hat{e}_x\left(z-z_2\right)dy\right]\Bigg\} \quad (15)$$

$$\overline{B_{\mathrm{Coil}.C}}=\oint\frac{\mu_0}{4\pi}\frac{NI_C\cos\left(\omega t+\theta_C\right)\overline{dl}\times\hat{r}_3}{r_3^2}$$
$$=\frac{\mu_0 NI_C\cos\left(\omega t+\theta_C\right)}{4\pi}$$
$$\times\oint\frac{\overline{dl}\times\left[\left(x-x_3\right)\hat{e}_x+\left(y-y_3\right)\hat{e}_y+\left(z-z_3\right)\hat{e}_z\right]}{\left(\left(x-x_1\right)^2+\left(y-y_1\right)^2+\left(z-z_1\right)^2\right)^{3/2}}$$
$$=\frac{\mu_0 NI_C\cos\left(\omega t+\theta_C\right)}{4\pi}$$
$$\times\Bigg\{\int_I\frac{1}{r_3^3}\left[\hat{e}_z\left(y-y_3\right)dx-\hat{e}_y\left(z-z_3\right)dx\right]$$
$$+\int_J\frac{1}{r_3^3}\left[-\hat{e}_z\left(x-x_3\right)dy-\hat{e}_x\left(z-z_3\right)dy\right]$$
$$+\int_K\frac{1}{r_3^3}\left[\hat{e}_z\left(y-y_3\right)dx-\hat{e}_y\left(z-z_3\right)dx\right]$$
$$+\int_L\frac{1}{r_3^3}\left[-\hat{e}_z\left(x-x_3\right)dy+\hat{e}_x\left(z-z_3\right)dy\right]\Bigg\} \quad (16)$$

where ω is the angular frequency of three independent currents. I_A, I_B, and I_C are the amplitudes of three independent currents, respectively. θ_A, θ_B, and θ_C are the phases of three independent currents, respectively. μ_0 is the permeability of vacuum, valued $4\pi\times10^{-7}\mathrm{N}\cdot\mathrm{A}^{-2}$.

According to (14)–(16), the B-field at $p(x,y,z)$ is the sum of the B-fields induced by coils A, B, and C as follows:

$$\begin{bmatrix}B_x\\B_y\\B_z\end{bmatrix}=\begin{bmatrix}B_x\\B_y\\B_z\end{bmatrix}_{\mathrm{Coil}.A}+\begin{bmatrix}B_x\\B_y\\B_z\end{bmatrix}_{\mathrm{Coil}.B}+\begin{bmatrix}B_x\\B_y\\B_z\end{bmatrix}_{\mathrm{Coil}.C}$$
$$=\begin{bmatrix}B_{x|A}+B_{x|C}+B_{x|E}+B_{x|F}+B_{x|G}+B_{x|H}\\+B_{x|J}+B_{x|L}\\B_{y|A}+B_{y|B}+B_{y|C}+B_{y|D}+B_{y|E}+B_{y|G}\\+B_{x|I}+B_{y|K}\\B_{z|B}+B_{Z|D}+B_{Z|F}+B_{z|H}+B_{Z|I}+B_{z|J}\\+B_{x|K}+B_{z|L}\end{bmatrix} \quad (17)$$

where $B_{m|n}$ is the B-field of m-axis component induced by contour n. The x-axis, y-axis, and z-axis components of B-field at $p(x,y,z)$ are listed in the Appendix.

IV. Field Orientation Based on Current Amplitude and Phase Control

In order to simplify the analysis of the B-field synthesis in the space, including the magnitude and direction, we have taken the geometric center of coils A, B, and C $p_o(0,0,0)$ as the example to discuss the B-field. From the Appendix, each axis component of the B-field at $p_o(0,0,0)$ is given as follows

$$\begin{cases}B_{x_{p_o}}=-\frac{\mu_0 NI_B\cos(\omega t+\theta_B)}{4\pi}\left(\frac{4bc}{b^2\sqrt{b^2+c^2}}+\frac{4bc}{c^2\sqrt{b^2+c^2}}\right)\\B_{y_{p_o}}=-\frac{\mu_0 NI_A\cos(\omega t+\theta_A)}{4\pi}\left(\frac{4ac}{a^2\sqrt{a^2+c^2}}+\frac{4ac}{c^2\sqrt{a^2+c^2}}\right)\\B_{z_{p_o}}=-\frac{\mu_0 NI_C\cos(\omega t+\theta_C)}{4\pi}\left(\frac{4ab}{a^2\sqrt{a^2+b^2}}+\frac{4ab}{b^2\sqrt{a^2+b^2}}\right).\end{cases} \quad (18)$$

The magnetic flux density induced by coils A, B, and C at any arbitrary point $p(x,y,z)$ can be expressed by using spherical coordinates

$$\begin{cases}R_p=\sqrt{B_x^2+B_y^2+B_z^2}\\\theta_p=\tan^{-1}\left(\sqrt{B_x^2+B_y^2}/B_z\right)\\\varphi_p=\tan^{-1}\left(B_y/B_x\right)\end{cases} \quad (19)$$

where R_p is the magnitude of the B-field at point p, θ_p is the angle between the zenith direction and the direction of the B-field, and φ_p is the signed angle measured from the azimuth reference direction to the orthogonal projection of the direction of the B-field on the reference plane ($R_p>0,\ 0\le\theta_p\le\pi,\ 0\le\varphi_p\le2\pi$).

Hence, according to (18) and (19), in order to simplify the analysis, the coils are assumed to be a square ($a=b=c=l$), and the magnetic flux density induced by coils A, B, and C at $p_o(0,0,0)$ is given by (20), shown at the bottom of this page.

The implementation using absolute values θ_A, θ_B, and θ_C is not convenient, so, for introducing the relative value to further reduce the equations, let $\theta_A=0$, $\theta_B-\theta_A=\Delta\theta_1$, $\theta_C-\theta_A=\Delta\theta_2$, as shown in (21) at the bottom of this page.

$$\begin{cases}R_{p_o}=\frac{\sqrt{2}\mu_0 N}{\pi l}\sqrt{I_A^2\cos^2\left(\omega t+\theta_A\right)+I_B^2\cos^2\left(\omega t+\theta_B\right)+I_C^2\cos^2\left(\omega t+\theta_C\right)}\\\theta_{p_o}=\tan^{-1}\left(-\sqrt{I_A^2\cos^2\left(\omega t+\theta_A\right)+I_B^2\cos^2\left(\omega t+\theta_B\right)}/I_C\cos\left(\omega t+\theta_C\right)\right)\\\varphi_{p_o}=\tan^{-1}\left(I_A\cos\left(\omega t+\theta_A\right)/I_B\cos\left(\omega t+\theta_B\right)\right)\end{cases} \quad (20)$$

$$\begin{cases}R_{p_o}=\frac{\sqrt{2}\mu_0 N}{\pi l}\sqrt{I_A^2\cos^2\left(\omega t\right)+I_B^2\cos^2\left(\omega t+\Delta\theta_1\right)+I_C^2\cos^2\left(\omega t+\Delta\theta_2\right)}\\\theta_{p_o}=\tan^{-1}\left(-\sqrt{I_A^2\cos^2\left(\omega t\right)+I_B^2\cos^2\left(\omega t+\Delta\theta_1\right)}/I_C\cos\left(\omega t+\Delta\theta_2\right)\right)\\\varphi_{p_o}=\tan^{-1}\left(I_A\cos\left(\omega t\right)/I_B\cos\left(\omega t+\Delta\theta_1\right)\right)\end{cases} \quad (21)$$

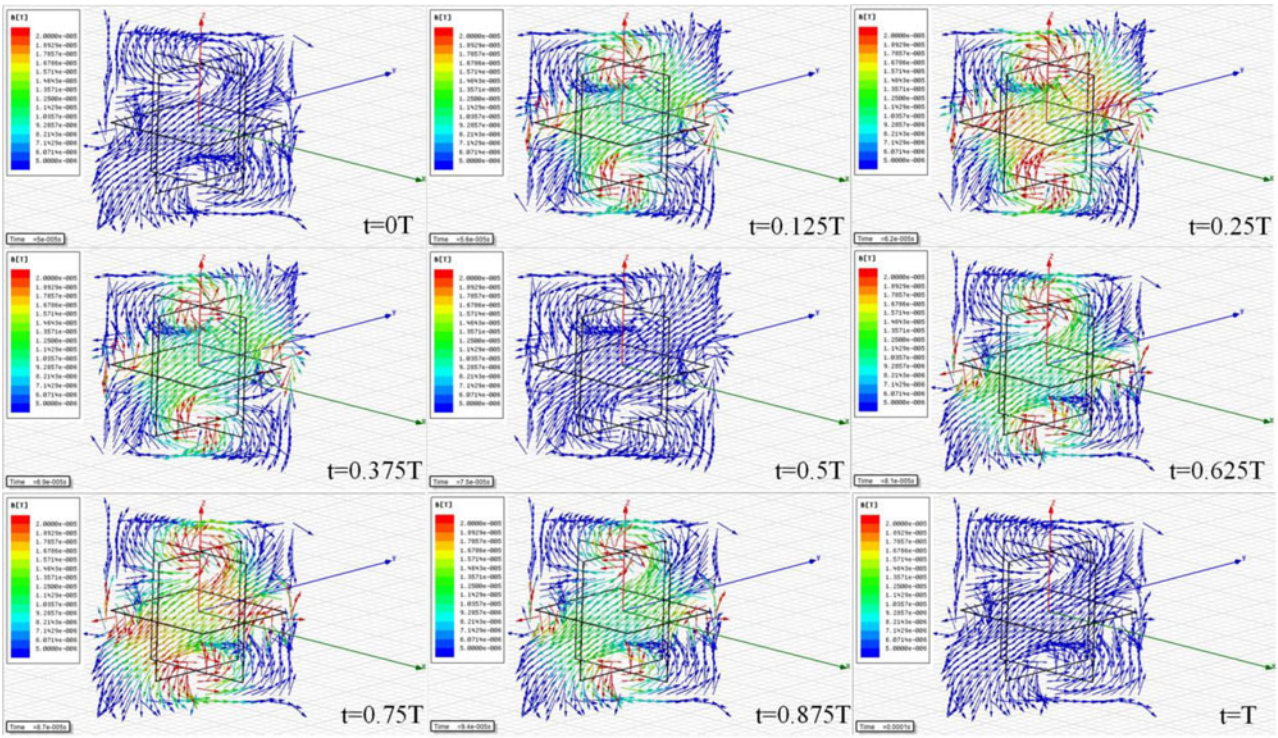

Fig. 3. Simulation results of shaped B-field at different times.

From the aforementioned equations, all the current amplitudes and phase angles I_A, I_B, I_C and θ_A, θ_B, θ_C, respectively, are the controllable variables. When the requirement of the B-field at point p_o is fulfilled, including the magnitude and direction of the B-field, a set of currents meeting the requirement can be solved.

For example, assume that the length of the side of each coil is 1 m, the number of turns of each coil is 10, and $\omega = 40\,000\pi$ rad/s, the requirements of the magnitude and direction of the B-field at $p_o(0,0,0)$ are $B_{(\text{amplitude})} = 10\,\mu\text{T}$, $\theta_{p_o} = 45°$, $\varphi_{p_o} = 45°$. The results can be solved: $I_A = 0.884$ A, $I_B = 0.884$ A, $I_C = 1.25$ A, $\Delta\theta_1 = 0$, and $\Delta\theta_2 = 0$. The coils are excited by three independent sources, and the sources are simulated by software "Maxwell Circuit Editor." The theoretical B-field can be simulated by using calculated values in software "Ansoft Maxwell," shown in Fig. 3, where $T = 50$ μs.

From Fig. 3, the B-field in the region of the proposed coils structure is shaped at $\theta = 45°$ and $\varphi = 45°$, when $t = 0.25$ T and $t = 0.75$ T, respectively, and the magnitude of the B-field achieves the maximum. Fig. 4 shows the trend of the B-field magnitude at point p_o from 0 to 100 μs. Within the error range allowed, the amplitude of the B-field is about 12 μT, which is close to the reference value 10 μT. All the simulation results agree with the theoretical results.

At the different requirements of B, θ, and φ, the following four specific conditions, including all the directions in the space, verify the proposed algorithm that realizes the 3-D full-range field orientation. The calculated values of amplitude and phase angle of currents are listed in Table I, where B_m means the amplitude of the B-field. The shaped B-fields under four conditions are shown in Fig. 5, when $t = 0.5$ T.

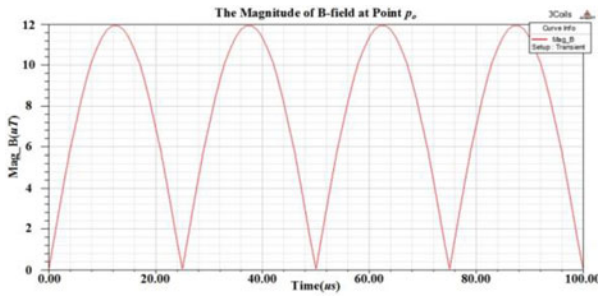

Fig. 4. Trend of B-field magnitude at point p_o.

TABLE I
REQUIREMENTS AND CALCULATED VALUES FOR DIFFERENT CONDITIONS

	Requirements			Calculated Values				
NO	B_m	θ	φ	I_A	I_B	I_C	$\Delta\theta_1$	$\Delta\theta_2$
1	10 μT	45°	45°	0.884 A	0.884 A	1.25 A	0°	0°
2	20 μT	45°	135°	1.768 A	1.768 A	2.5 A	180°	0°
3	10 μT	135°	45°	0.884 A	0.884 A	1.25 A	0°	180°
4	20 μT	135°	135°	1.768 A	1.768 A	2.5 A	180°	180°

From above-mentioned analysis, a universal conclusion can be achieved, which will provide a criterion for further application. The whole space, taking the geometric center of the proposed coils structure as origin, can be divided into eight

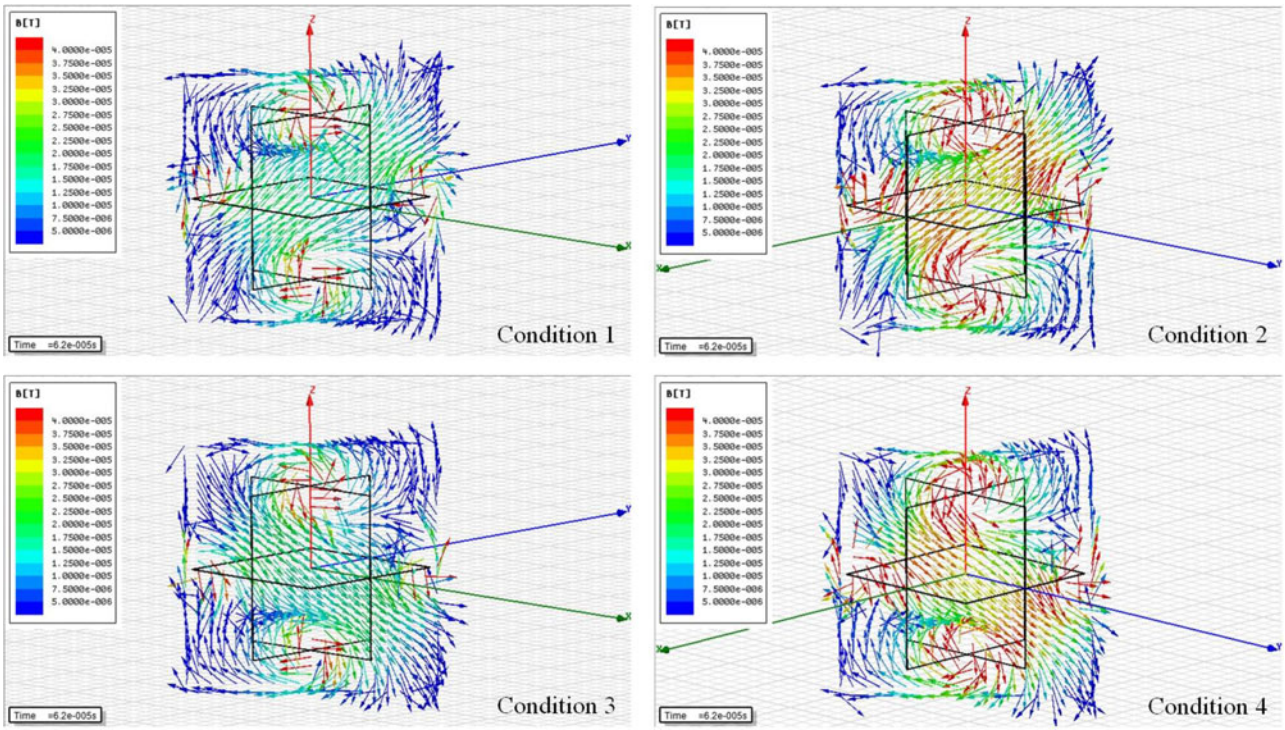

Fig. 5. Shaped B-fields under four conditions.

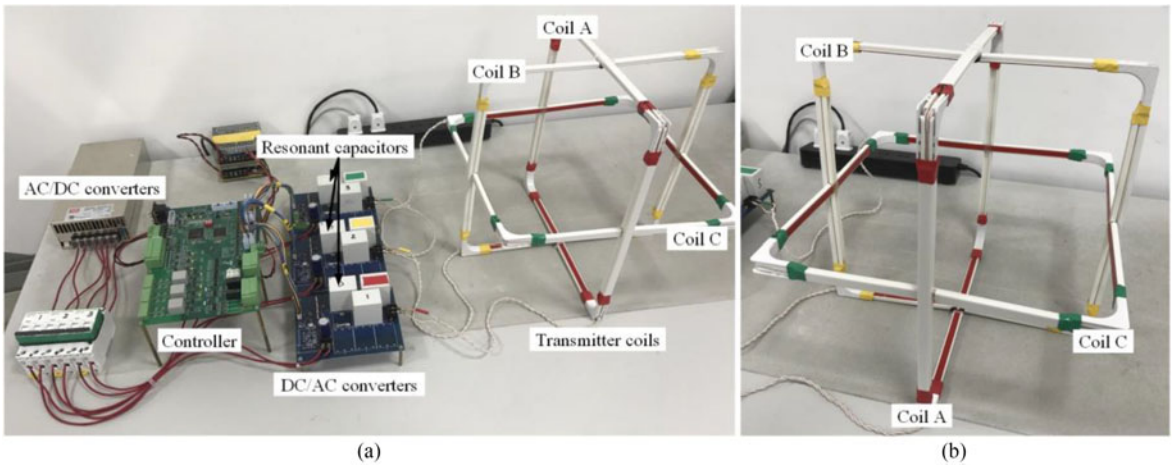

Fig. 6. 3-D field orientation WPT system. (a) Prototype of the 3-D field orientation WPT system. (b) Detailed structure of three transmitter coils.

sections. Considering the B-field is alternating, the eight sections can be further grouped into the following four regions:

1) $x > 0, y > 0, z > 0$ and $x < 0, y < 0, z < 0$;
2) $x > 0, y\langle 0, z\rangle 0$ and $x\langle 0, y\rangle 0, z < 0$;
3) $x\langle 0, y\rangle 0, z > 0$ and $x > 0, y < 0, z < 0$;
4) $x < 0, y\langle 0, z\rangle 0$ and $x > 0, y > 0, z < 0$.

When the receiver coil is located in region 1), θ and φ are given as constant, $0 \le \theta < \pi/2,\ 0 \le \varphi < \pi/2$ (or $\pi/2 \le \theta \le \pi,\ \pi \le \varphi < 3\pi/2\ \pi/2 \le \theta \le \pi,\ \pi \le \varphi < 3\pi/2$); only when $\Delta\theta_1 = 0$ and $\Delta\theta_2 = 0$ can the second and third equations of (21) have the effective and physically realizable solutions of $I_A,\ I_B,$ and I_C. Similarly, when the receiver coil is located in regions 2), 3), and 4), $0 \le \theta < \pi/2,\ \ 3\pi/2 \le \varphi \le 2\pi$ (or $\pi/2 \le \theta \le \pi,\ \ \pi/2 \le \varphi < \pi$), $0 \le \theta < \pi/2,\ \ \pi/2 \le \varphi < \pi$ (or $\pi/2 \le \theta \le \pi,\ \ 3\pi/2 \le \varphi \le 2\pi$) and $0 \le \theta < \pi/2,\ \ \pi \le \varphi < 3\pi/2$ (or $\pi/2 \le \theta \le \pi,\ \ 0 \le \varphi < \pi/2$), respectively; only when $\Delta\theta_1$ and $\Delta\theta_2$ are 180° and 180°, 180° and 0°, 0° and 180°, respectively, can the second and third equations of (21) have the effective and physically realizable solutions of $I_A,\ I_B,$ and I_C. So, when the receiver coil(s) are located in regions 1), 2), 3), and 4), respectively, $\Delta\theta_1$ and $\Delta\theta_2$ are accordingly set as 0° and 0°, 180° and 180°, 180° and 0°, 0° and 180°, respectively. According to the location of receiver coil(s), the current phase angles can be first decided and a rough field orientation is completed.

TABLE II
ACTUAL COIL PARAMETERS OF THE 3-D FIELD ORIENTATION WPT SYSTEM

Coil	Frequency (kHz)	L (μH)	C (μF)	R (mΩ)	Length of Side (mm)	Turns	Wire Radius (mm)
Coil A (red)	19.517	10.06	6.61	50.23	328	3	2.2
Coil B (yellow)	19.518	10.09	6.59	50.30	328	3	2.2
Coil C (green)	19.513	10.11	6.58	50.43	328	3	2.2
Coil	Frequency (kHz)	L (μH)	C (μF)	R (mΩ)	Diameter (mm)	Turns	Wire Radius (mm)
Receiver coil	19.609	15.61	4.22	43.10	276	5	2.2

TABLE III
PARAMETERS OF THREE CASES FOR SHAPED MAGNETIC FIELD MEASUREMENTS

Case	I_{A_rms}	I_{B_rms}	I_{C_rms}	$\Delta\theta_1$	$\Delta\theta_2$
I. $\theta = 45°, \varphi = 45°$	7.07 A	7.07 A	10 A	0	0
II. $\theta = 55°, \varphi = 45°$	8.16 A	8.16 A	8.16 A	0	0
III. $\theta = 45°, \varphi = 135°$	7.07 A	7.07 A	10 A	180°	0

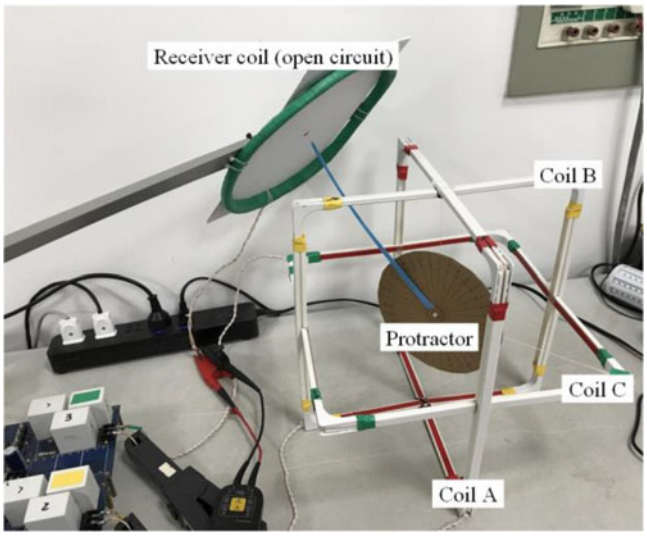

Fig. 7. Implementation of shaped magnetic field measurements.

Then, the magnitude of the B-field and further precise field orientation are realized by the current amplitude control. For example, when $\theta = 30°$, $\varphi = 60°$, the field orientation locates in region 1), and $\Delta\theta_1$ and $\Delta\theta_2$ are set as $0°$ and $0°$, respectively, hence the following equations will be derived:

$$\begin{cases} (I_A^2 + I_B^2)/I_C^2 = \tan^2(30°) \\ I_A/I_B = \tan(60°). \end{cases} \tag{22}$$

From (22), $I_A = I_C/2$ and $I_B = \sqrt{3}I_C/6$. Then, according to the reference magnitude of the B-field, the following equation is obtained:

$$B_{\text{ref}} = \frac{\sqrt{2}\mu_0 N}{\pi l}\sqrt{I_A^2\cos^2(\omega t) + I_B^2\cos^2(\omega t) + I_C^2\cos^2(\omega t)}. \tag{23}$$

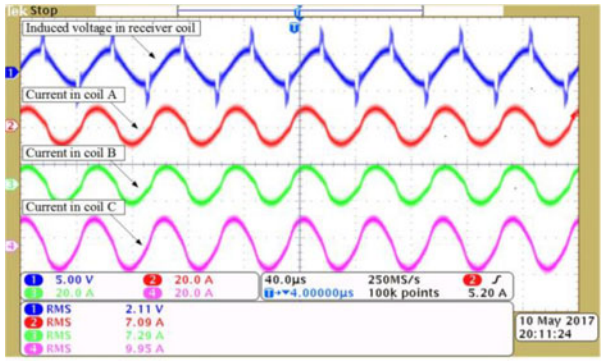

(a)

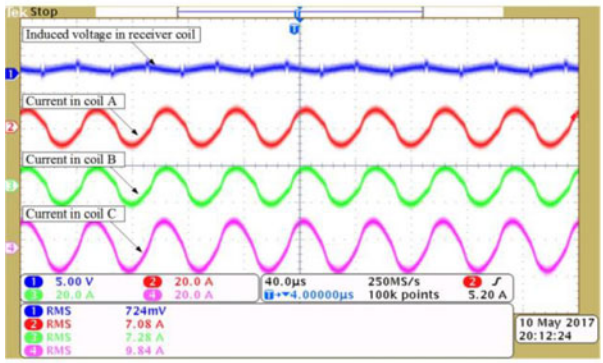

(b)

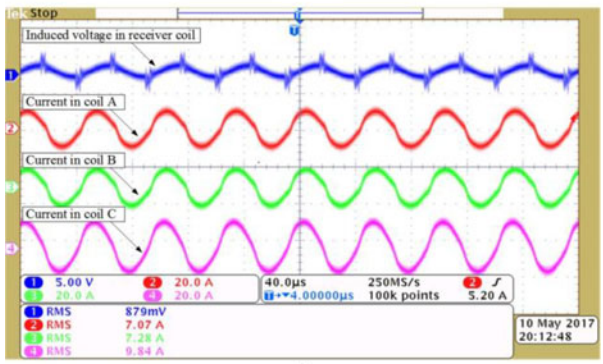

(c)

Fig. 8. Waveforms in case I. (a) Waveforms of $\theta = 45°$, $\varphi = 45°$. (b) Waveforms of $\theta = 45°$, $\varphi = 135°$. (c) Waveforms of $\theta = 45°$, $\varphi = 225°$.

From (23), the actual value of I_A, I_B, and I_C can be solved. The whole steps of the proposed field orientation technique are done. In practical application, the solutions I_A, I_B, I_C, $\Delta\theta_1$, and $\Delta\theta_2$ can be applied, and the shaped B-field will be formed.

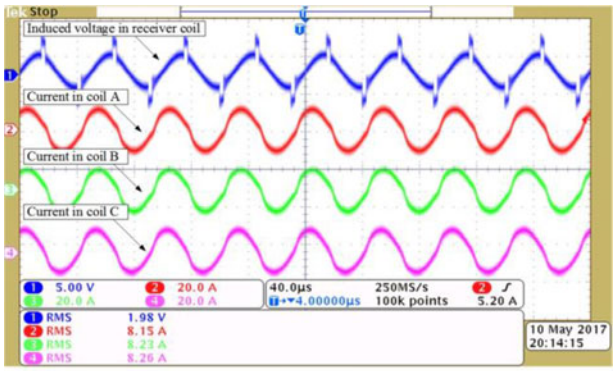

(a)

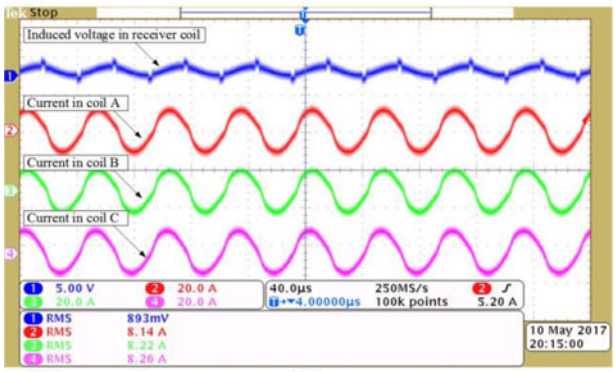

(b)

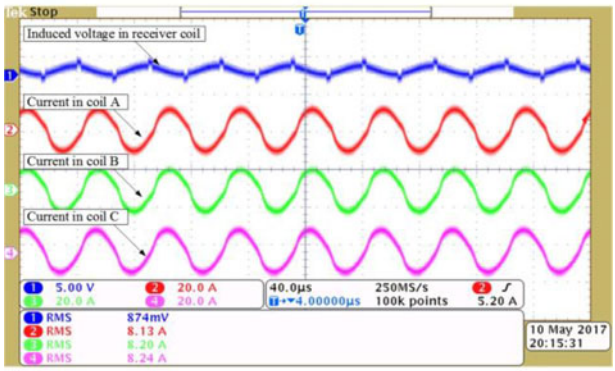

(c)

Fig. 9. Waveforms in case II. (a) Waveforms of $\theta = 55°$, $\varphi = 45°$. (b) Waveforms of θ=0, φ=45°. (c) Waveforms of θ=90°, $\varphi = 45°$.

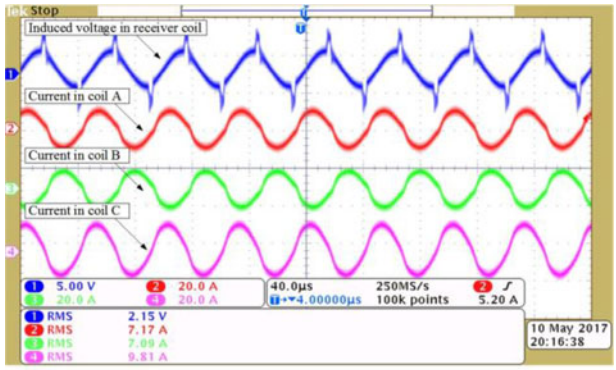

(a)

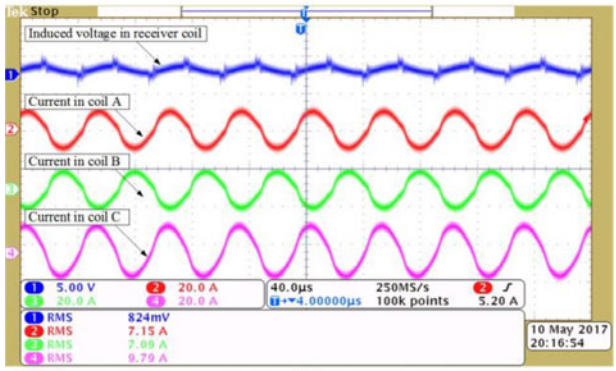

(b)

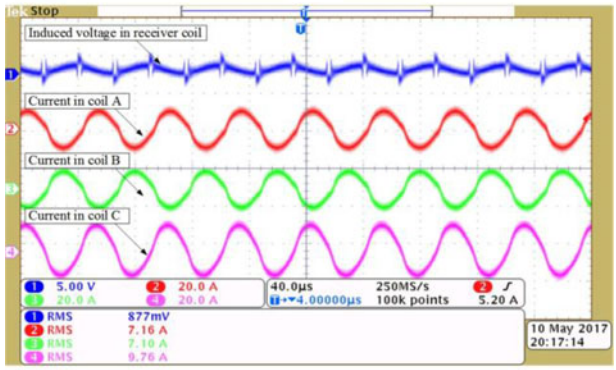

(c)

Fig. 10. Waveforms in case III. (a) Waveforms of $\theta = 45°$, $\varphi = 135°$. (b) Waveforms of θ=45°, φ=225°. (c) Waveforms of θ=45°, $\varphi = 315°$.

V. Hardware Implementation and Experimental Results

Based on the previous theoretical analysis, a 3-D field orientation WPT system is implemented, which is shown in Fig. 6. Fig. 6(a) shows the prototype of a 3-D field orientation WPT system, which is composed of a controller equipped with a floating-point digital signal processor (DSP, TMS320F28335) and a field programmable gate array (FPGA, EP2C8J144C8N), an ac/dc converter with three independent channel 12 V output, three independent controllable dc/ac converters, three independent resonance tanks, including series resonant capacitors and transmitter coils, one receiver coil connected with series resonant capacitor and resistance load. The inductance of each transmitter coil is designed as 10 μH, the inductance of the receiver coil is designed as 15.6 μH, the capacitance of each series resonant capacitor for the transmitter is designed as 6.6 μF, the capacitance of the series resonant capacitor for the receiver is designed as 4.23 μF, the frequency of ac voltage generated by dc/ac converters is designed as 19.59 kHz, DSP is in charge of mathematical calculation, and FPGA is in charge of generating pulse width modulation signals for switches. Fig. 6(b) shows the detailed structure of three transmitter coils, including coil A labeled red, coil B labeled yellow, and coil C labeled green, each coil is a square with the length of side 328 mm, each coil has three turns of Litz wire with radius 2.2 mm. The actual coil parameters of the 3-D field orientation WPT system are presented in Table II.

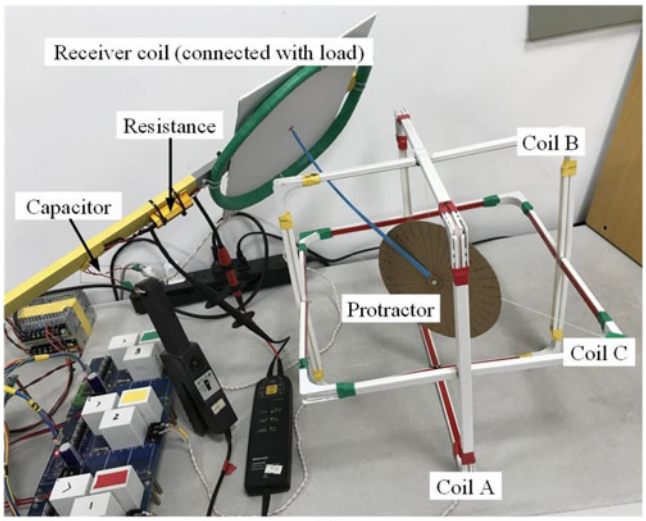

(a)

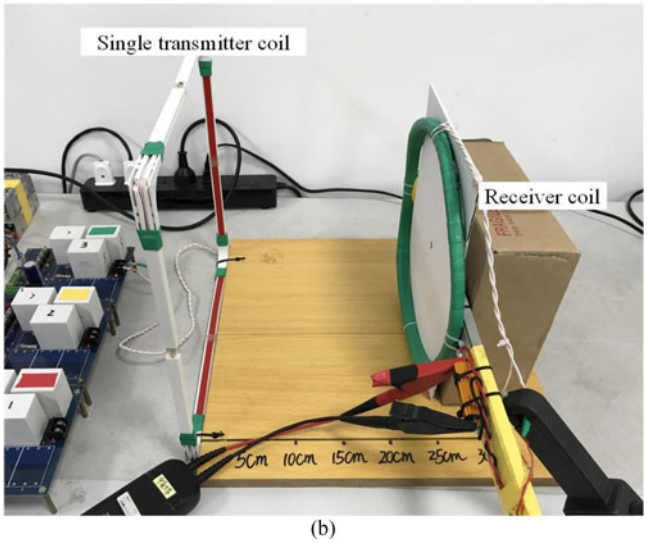

(b)

Fig. 11. Experimental setups used for measuring the energy transfer efficiency. (a) The setup for case I. (b) The setup for case II.

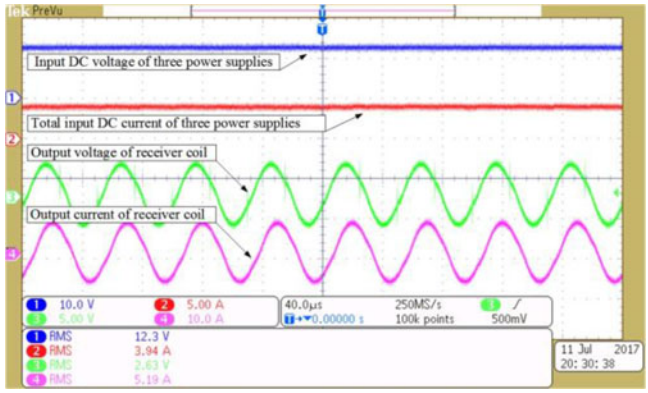

Fig. 12. Waveforms in case I.

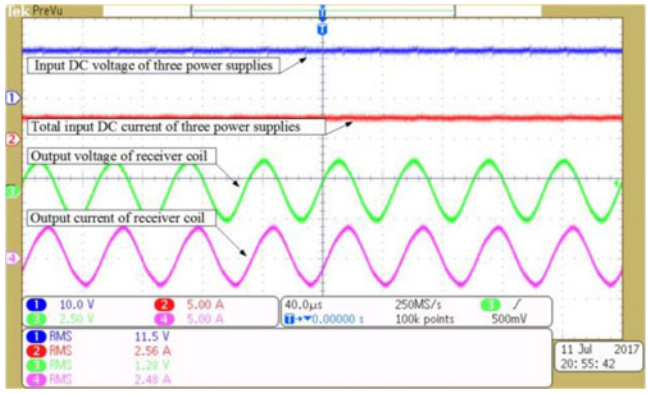

Fig. 13. Waveforms in case II.

The experimental results of the implemented 3-D field orientation WPT system are presented below. In order to further verify the previous theoretical analysis, two sets of experiments are carried out, shaped magnetic field measurements and energy transfer efficiency measurements.

For shaped magnetic field measurements, it is not easy to directly measure the magnetic flux density; hence, we used the induced electromotive force induced in the receiver coil to indirectly measure the shaped magnetic field in the region of the receiver coil. The following cases are set to compare the magnetic field pointing to the receiver coil and the magnetic field not pointing to the receiver coil, which are presented in Table III. The distance between the center of receiver coil and the center of three transmitter coils remains constant, i.e., 30 cm. The plane of receiver coil is perpendicular to the line from the center of receiver coil and the center of three transmitter coils. The experimental results of each case include the induced electromotive force when the receiver coil is located in the given direction and the induced electromotive force when the receiver coil is not located in the given direction. The implementation in shaped magnetic field measurements is shown in Fig. 7.

In case I, $I_{A\_\mathrm{rms}} = 7.07$ A, $I_{B\_\mathrm{rms}} = 7.07$ A, $I_{C\_\mathrm{rms}} = 10$ A, $\Delta\theta_1 = 0$, and $\Delta\theta_2 = 0$. First, let the receiver coil be at $\theta = 45°$, $\varphi = 45°$, then let the receiver coil be at $\theta = 45°$, $\varphi = 135°$ and $\theta = 45°$, $\varphi = 225°$, respectively. As shown in Fig. 8, from top to bottom in each figure, the waveforms are the induced voltage in the receiver coil, the current in coil A, the current in coil B and, the current in coil C.

In case II, $I_{A\_\mathrm{rms}} = 8.16$ A, $I_{B\_\mathrm{rms}} = 8.16$ A, $I_{C\_\mathrm{rms}} = 8.16$ A, $\Delta\theta_1 = 0$, and $\Delta\theta_2 = 0$. First, let the receiver coil be at $\theta = 55°$, $\varphi = 45°$, then let the receiver coil be at $\theta = 0$, $\varphi = 45°$ and $\theta = 90°$, $\varphi = 45°$, respectively. As shown in Fig. 9, from top to bottom in each figure, the waveforms are the induced voltage in the receiver coil, the current in coil A, the current in coil B, and the current in coil C.

In case III, $I_{A\_\mathrm{rms}} = 7.07$ A, $I_{B\_\mathrm{rms}} = 7.07$ A, $I_{C\_\mathrm{rms}} = 10$ A, $\Delta\theta_1 = 180°$, and $\Delta\theta_2 = 0$. First, let the receiver coil be at $\theta = 45°$, $\varphi = 135°$, then, let the receiver coil be at $\theta = 45°$, $\varphi = 225°$ and $\theta = 45°$, $\varphi = 315°$, respectively. As shown in Fig. 10, from top to bottom in each figure, the waveforms are

the induced voltage in the receiver coil, the current in coil A, the current in coil B, and the current in coil C.

From the aforementioned experimental results, the magnetic field is shaped according to expected direction, and the magnetic field is concentrated at a certain direction. Comparing case I with case II, when $\Delta\theta_1$ and $\Delta\theta_2$ remain unchanged, changing the relative values of I_{A_rms}, I_{B_rms}, and I_{C_rms}, and keeping the sum of squares of I_{A_rms}, I_{B_rms}, andI_{C_rms} constant, the direction of shaped magnetic field changes from $\theta = 45^\circ$ to $\theta = 55^\circ$. Comparing case I with case III, when I_A, I_B, and I_C remain unchanged, changing $\Delta\theta_1$ and $\Delta\theta_2$, the region of shaped magnetic field changes from region 1) to region 3).

For energy transfer efficiency measurements, the load of receiver coil is a resistance $0.5\ \Omega$. In order to explain the improvements of energy transfer efficiency, two experiments are carried out with the following: case I—three transmitter coils and one receiver coil; case II—one transmitter coil and one receiver coil. In both cases, the initial magnitude of magnetic field at the center is equally set same for comparison, which means the currents of three transmitter coils in case I is $\sqrt{3}/3$ of the current of the single transmitter coil in case II. The receiver coil is placed vertically with the direction of shaped magnetic field. The distance from the center of three transmitter coils to the center of receiver coil in case I is along with the direction of magnetic field in the center of three transmitter coils, the distance from the center of one transmitter coil to the center of receiver coil in case II is along with the direction of magnetic field in the center of one transmitter coil, and both the distances are set as 25 cm. The experimental setups used for measuring the energy transfer efficiency are shown in Fig. 11, where Fig. 11(a) is for case I and Fig. 11(b) is for case II.

In case I, $I_{A\_\mathrm{rms}} = 10\,\mathrm{A}$, $I_{B\_\mathrm{rms}} = 10\,\mathrm{A}$, $I_{C\_\mathrm{rms}} = 10\,\mathrm{A}$, $\Delta\theta_1 = 0$, and $\Delta\theta_2 = 0$. As shown in Fig. 12, from top to bottom, the waveforms are the input dc voltage of three power supplies, the total input dc current of three power supplies, the output voltage of receiver coil, and the output current of receiver coil.

In case II, $I_{A\_\mathrm{rms}} = 0\,\mathrm{A}$, $I_{B\_\mathrm{rms}} = 0\,\mathrm{A}$, $I_{C\_\mathrm{rms}} = 17.32\,\mathrm{A}$, $\Delta\theta_1 = 0$, and $\Delta\theta_2 = 0$. As shown in Fig. 13, from top to bottom, the waveforms are the input dc voltage of single power supply, the input dc current of single power supply, the output voltage of receiver coil, and the output current of receiver coil.

From the aforementioned results, the proposed magnetic field orientation method improves the energy transfer efficiency and offers larger effective transmission distance when the power needed in the receiver coil is given. Comparing case I and case II, when the distances and the sum of squares of I_A, I_B, andI_C remain the same in the two cases, the output voltage of receiver coil in case I is larger than the output voltage of receiver coil in case II, which means when the expected output voltage of receiver coil is given, the proposed three transmitter coils structure has longer transmission distance, the energy transfer capacity of the proposed magnetic field orientation method is better than that of the conventional method. Similarly, in this group of experiments, the efficiency is equal to the ratio of the load power and the input dc power. According to Figs. 12 and 13, the load power and efficiency of the proposed magnetic field orientation method are about 13.7 W and 28.2%, respectively, and the load power and efficiency of the conventional method are about 3.2 W and 10.8%, respectively. For the result of efficiency of the conventional method, because the calculated efficiency includes the loss of a dc/ac converter, when the required current becomes larger, the loss of a dc/ac converter will become larger. Meanwhile, because the given transfer distance 25 cm is relatively large compared with the size of transmitter coil, when just single transmitter coil works, the excited magnetic field will sharply diverge and some energy will be wasted. Hence, the single transmitter coil structure will lead to lower efficiency when the distance highly increases. However, the proposed three transmitter coils structure can reduce the requirement of current flowing in one transmitter coil and shape the magnetic field to reduce unnecessary energy waste, which will obviously improve the energy transfer efficiency compared with the conventional single transmitter coil structure. Generally, the proposed 3-D magnetic field orientation method can effectively improve the performance of a WPT system.

VI. Conclusion

This paper introduced a universal algorithm to realize 3-D full-range field orientation to adjust the magnitude and direction of the B-field at an arbitrary point. The B-field is concentrated in a beam with reduced leakage magnetic flux, consequently, the power transfer efficiency and distance are effectively improved. The proposed algorithm is very useful to guide practical 3-D WPT system design with more flexible coupling tolerance. The analytical, simulation, and experimental results obtained from this research demonstrate that if the mathematic relationships between the B-filed generated by the transmitter and the power received by the receiver are established, together with orientation and power closed-loop accurate steady-state controls, the whole 3-D WPT system will be able to eliminate the steady-state error, have certain ability of anti-interference, and achieve more precise power transfer and direction orientation to targeted loads.

Appendix

The x-axis, y-axis, and z-axis components of the B-field at $p(x, y, z)$ are listed in Table IV, where B_m is the B-field of the m-axis in the space, and $B_m|_{\mathrm{Coil}\ N}$ is the B-field of the m-axis component induced by coil N.

TABLE IV

x-AXIS, *y*-AXIS, AND *z*-AXIS COMPONENTS OF B-FIELD AT $p(x, y, z)$

B_m	$B_m\|_{\text{Coil } N}$	Value
B_x	$B_x\|_{\text{Coil } A}$	$\frac{\mu_0 N I_A \cos(\omega t+\theta_A)}{4\pi}\left\{\left(\frac{y(z-c)}{[(x-a)^2+y^2][(x-a)^2+y^2+(z-c)^2]^{\frac{1}{2}}}-\frac{y(z+c)}{[(x-a)^2+y^2][(x-a)^2+y^2+(z+c)^2]^{\frac{1}{2}}}\right)+\left(\frac{y(z+c)}{[(x+a)^2+y^2][(x+a)^2+y^2+(z+c)^2]^{\frac{1}{2}}}-\frac{y(z-c)}{[(x+a)^2+y^2][(x+a)^2+y^2+(z-c)^2]^{\frac{1}{2}}}\right)\right\}$
	$B_x\|_{\text{Coil } B}$	$\frac{\mu_0 N I_B \cos(\omega t+\theta_B)}{4\pi}\left\{\left(\frac{(y+b)(z-c)}{[x^2+(y+b)^2][x^2+(y+b)^2+(z-c)^2]^{\frac{1}{2}}}-\frac{(y+b)(z+c)}{[x^2+(y+b)^2][x^2+(y+b)^2+(z+c)^2]^{\frac{1}{2}}}\right)+\left(\frac{(y+b)(z-c)}{[x^2+(z-c)^2][x^2+(y+b)^2+(z-c)^2]^{\frac{1}{2}}}-\frac{(y-b)(z-c)}{[x^2+(z-c)^2][x^2+(y-b)^2+(z-c)^2]^{\frac{1}{2}}}\right)+\left(\frac{(y-b)(z+c)}{[x^2+(y-b)^2][x^2+(y-b)^2+(z+c)^2]^{\frac{1}{2}}}-\frac{(y-b)(z-c)}{[x^2+(y-b)^2][x^2+(y-b)^2+(z-c)^2]^{\frac{1}{2}}}\right)+\left(\frac{(y-b)(z+c)}{[x^2+(z+c)^2][x^2+(y-b)^2+(z+c)^2]^{\frac{1}{2}}}-\frac{(y+b)(z+c)}{[x^2+(z+c)^2][x^2+(y+b)^2+(z+c)^2]^{\frac{1}{2}}}\right)\right\}$
	$B_x\|_{\text{Coil } C}$	$\frac{\mu_0 N I_C \cos(\omega t+\theta_C)}{4\pi}\left\{\left(\frac{(y+b)z}{[(x+a)^2+z^2][(x+a)^2+(y+b)^2+z^2]^{\frac{1}{2}}}-\frac{(y-b)z}{[(x+a)^2+z^2][(x+a)^2+(y-b)^2+z^2]^{\frac{1}{2}}}\right)+\left(\frac{(y-b)z}{[(x-a)^2+z^2][(x-a)^2+(y-b)^2+z^2]^{\frac{1}{2}}}-\frac{(y+b)z}{[(x-a)^2+z^2][(x-a)^2+(y+b)^2+z^2]^{\frac{1}{2}}}\right)\right\}$
B_y	$B_y\|_{\text{Coil } A}$	$\frac{\mu_0 N I_A \cos(\omega t+\theta_A)}{4\pi}\left\{\left(\frac{(x-a)(z+c)}{[(x-a)^2+y^2][(x-a)^2+y^2+(z+c)^2]^{\frac{1}{2}}}-\frac{(x-a)(z-c)}{[(x-a)^2+y^2][(x-a)^2+y^2+(z-c)^2]^{\frac{1}{2}}}\right)+\left(\frac{(x+a)(z-c)}{[y^2+(z-c)^2][(x+a)^2+y^2+(z-c)^2]^{\frac{1}{2}}}-\frac{(x-a)(z-c)}{[y^2+(z-c)^2][(x-a)^2+y^2+(z-c)^2]^{\frac{1}{2}}}\right)+\left(\frac{(x+a)(z-c)}{[(x+a)^2+y^2][(x+a)^2+y^2+(z-c)^2]^{\frac{1}{2}}}-\frac{(x+a)(z+c)}{[(x+a)^2+y^2][(x+a)^2+y^2+(z+c)^2]^{\frac{1}{2}}}\right)+\left(\frac{(x-a)(z+c)}{[y^2+(z+c)^2][(x-a)^2+y^2+(z+c)^2]^{\frac{1}{2}}}-\frac{(x+a)(z+c)}{[y^2+(z+c)^2][(x+a)^2+y^2+(z+c)^2]^{\frac{1}{2}}}\right)\right\}$
	$B_y\|_{\text{Coil } B}$	$\frac{\mu_0 N I_B \cos(\omega t+\theta_B)}{4\pi}\left\{\left(\frac{x(z+c)}{[x^2+(y+b)^2][x^2+(y+b)^2+(z+c)^2]^{\frac{1}{2}}}-\frac{x(z-c)}{[x^2+(y+b)^2][x^2+(y+b)^2+(z-c)^2]^{\frac{1}{2}}}\right)+\left(\frac{x(z-c)}{[x^2+(y-b)^2][x^2+(y-b)^2+(z-c)^2]^{\frac{1}{2}}}-\frac{x(z+c)}{[x^2+(y-b)^2][x^2+(y-b)^2+(z+c)^2]^{\frac{1}{2}}}\right)\right\}$
	$B_y\|_{\text{Coil } C}$	$\frac{\mu_0 N I_C \cos(\omega t+\theta_C)}{4\pi}\left\{\left(\frac{(x+a)z}{[(y+b)^2+z^2][(x+a)^2+(y+b)^2+z^2]^{\frac{1}{2}}}-\frac{(x-a)z}{[(y+b)^2+z^2][(x-a)^2+(y+b)^2+z^2]^{\frac{1}{2}}}\right)+\left(\frac{(x-a)z}{[(y-b)^2+z^2][(x-a)^2+(y-b)^2+z^2]^{\frac{1}{2}}}-\frac{(x+a)z}{[(y-b)^2+z^2][(x+a)^2+(y-b)^2+z^2]^{\frac{1}{2}}}\right)\right\}$
B_z	$B_z\|_{\text{Coil } A}$	$\frac{\mu_0 N I_A \cos(\omega t+\theta_A)}{4\pi}\left\{\left(\frac{(x-a)y}{[y^2+(z-c)^2][(x-a)^2+y^2+(z-c)^2]^{\frac{1}{2}}}-\frac{(x+a)y}{[y^2+(z-c)^2][(x+a)^2+y^2+(z-c)^2]^{\frac{1}{2}}}\right)+\left(\frac{(x+a)y}{[y^2+(z+c)^2][(x+a)^2+y^2+(z+c)^2]^{\frac{1}{2}}}-\frac{(x-a)y}{[y^2+(z+c)^2][(x-a)^2+y^2+(z+c)^2]^{\frac{1}{2}}}\right)\right\}$
	$B_z\|_{\text{Coil } B}$	$\frac{\mu_0 N I_B \cos(\omega t+\theta_B)}{4\pi}\left\{\left(\frac{x(y-b)}{[x^2+(z-c)^2][x^2+(y-b)^2+(z-c)^2]^{\frac{1}{2}}}-\frac{x(y+b)}{[x^2+(z-c)^2][x^2+(y+b)^2+(z-c)^2]^{\frac{1}{2}}}\right)+\left(\frac{x(y+b)}{[x^2+(z+c)^2][x^2+(y+b)^2+(z+c)^2]^{\frac{1}{2}}}-\frac{x(y-b)}{[x^2+(z+c)^2][x^2+(y-b)^2+(z+c)^2]^{\frac{1}{2}}}\right)\right\}$
	$B_z\|_{\text{Coil } C}$	$\frac{\mu_0 N I_C \cos(\omega t+\theta_C)}{4\pi}\left\{\left(\frac{(x-a)(y+b)}{[(y+b)^2+z^2][(x-a)^2+(y+b)^2+z^2]^{\frac{1}{2}}}-\frac{(x+a)(y+b)}{[(y+b)^2+z^2][(x+a)^2+(y+b)^2+z^2]^{\frac{1}{2}}}\right)+\left(\frac{(x+a)(y-b)}{[(x+a)^2+z^2][(x+a)^2+(y-b)^2+z^2]^{\frac{1}{2}}}-\frac{(x+a)(y+b)}{[(x+a)^2+z^2][(x+a)^2+(y+b)^2+z^2]^{\frac{1}{2}}}\right)+\left(\frac{(x+a)(y-b)}{[(y-b)^2+z^2][(x+a)^2+(y-b)^2+z^2]^{\frac{1}{2}}}-\frac{(x-a)(y-b)}{[(y-b)^2+z^2][(x-a)^2+(y-b)^2+z^2]^{\frac{1}{2}}}\right)+\left(\frac{(x-a)(y+b)}{[(x-a)^2+z^2][(x-a)^2+(y+b)^2+z^2]^{\frac{1}{2}}}-\frac{(x-a)(y-b)}{[(x-a)^2+z^2][(x-a)^2+(y-b)^2+z^2]^{\frac{1}{2}}}\right)\right\}$

References

[1] A. Kurs, A. Karalis, J. D. Joannopoulos, and M. Soljacic, "Wireless power transfer via strongly coupled magnetic resonance," *Science*, vol. 317, no. 5834, pp. 83–86, Jul. 2007, doi: 10.1126/science.1143254.

[2] A. Karalis, J. D. Joannopoulos, and M. Soljacic, "Efficiency wireless nonradiative mid-range energy transfer," *Ann. Phys.*, vol. 323, pp. 34–48, Jan. 2008, doi: 10.1016/j.aop.2007.04.017.

[3] S. L. Ho, J. Wang, W. N. Fu, and M. Sun, "A comparative study between novel witricity and traditional inductive magnetic coupling in wireless charging," *IEEE Trans. Magn.*, vol. 47, no. 5, pp. 1522–1525, May 2011, doi: 10.1109/TMAG.2010.2091495.

[4] A. P. Sample, D. T. Meyer, and J. R. Smith, "Analysis experimental results, and range adaptation of magnetically coupled resonators for wireless power transfer," *IEEE Trans. Ind. Electron.*, vol. 58, no. 2, pp. 544–554, Feb. 2011, doi: 10.1109/TIE.2010.2046002.

[5] S. Y. R. Hui, W. X. Zhong, and C. K. Lee, "A critical review of recent progress in mid-range wireless power transfer," *IEEE Trans. Power Electron.*, vol. 29, no. 9, pp. 4500–4511, Sep. 2014, doi: 10.1109/TPEL.2013.2249670.

[6] T. Imura, "Equivalent circuit for repeater coil for wireless power transfer via magnetic resonant coupling considering signed coupling," in *Proc. IEEE Ind. Electron. Appl. Conf.*, 2011, pp. 1501–1506, doi: 10.1109/ICIEA.2011.5975828.

[7] J. Kim, H. Son, K. Kim, and Y. Park, "Efficiency analysis of magnetic resonance wireless power transfer with intermediate resonance coil," *IEEE Coils Wireless Propag. Lett.*, vol. 10, pp. 389–392, May 2011, doi: 10.1109/LAWP.2011.2150192.

[8] Y. Moriwaki, T. Imura, and Y. Hori, "Basic study on reduction of reflected power using DC/DC converters in wireless power transfer system via magnetic resonant coupling," in *Proc. Telecommun. Energy Conf.*, 2011, pp. 1–5, doi: 10.1109/INTLEC.2011.6099737.

[9] Y. Lim, H. Tang, S. Lim, and J. Park, "An adaptive impedance-matching network based on a novel capacitor matrix for wireless power transfer," *IEEE Trans. Power Electron.*, vol. 29, no. 8, pp. 4403–4413, Aug. 2014, doi: 10.1109/TPEL.2013.2292596.

[10] C. K. Lee, W. X. Zhong, and S. Y. R. Hui, "Effect of magnetic coupling of nonadjacent resonators on wireless power domino-resonator systems," *IEEE Trans. Power Electron.*, vol. 27, no. 4, pp. 1905–1916, Apr. 2012, doi: 10.1109/TPEL.2011.2169460.

[11] B. H. Waters, A. P. Sample, and J. R. Smith, "Adaptive impedance matching for magnetically coupled resonators," in *Proc. Prog. Electromagn. Res. Symp.*, Moscow, Russia, Aug. 2012, pp. 694–701.

[12] R. Johari, J. V. Krogmeier, and D. J. Love, "Analysis and practical considerations in implementing multiple transmitters for wireless power transfer via coupled magnetic resonance," *IEEE Trans. Ind. Electron.*, vol. 61, no. 4, pp. 1774–1783, Apr. 2014, doi: 10.1109/TIE.2013.2263780.

[13] W. Ahn *et al.*, "Design of coupled resonators for wireless power transfer to mobile devices using magnetic field shaping," in *Proc. IEEE Int. Symp. Electromagn. Compat.*, 2012, pp. 772–776, doi: 10.1109/ISEMC.2012.6351667.

[14] S. Santalunai, C. Thongsopa, and T. Thosdeekoraphat, "An increasing the power transmission efficiency of flat spiral coils by using ferrite materials for wireless power transfer applications," in *Proc. Int. Conf. Electr. Eng./Electron. Comput. Telecommun. Inf. Technol.*, 2014, pp. 1–4, doi: 10.1109/ECTICon.2014.6839838.

[15] Y. Lim and J. Park, "A novel phase-control-based energy beamforming techniques in nonradiative wireless power transfer," *IEEE Trans. Power Electron.*, vol. 30, no. 11, pp. 6274–6287, Nov. 2015, doi: 10.1109/TPEL.2014.2379672.

Qi Zhu (GS'16) was born in Anhui, China, in 1993. He received the B.S. degree in electrical engineering and automation from the Central South University, Changsha, China, in 2014, where he is currently working toward the Ph.D. degree in electrical engineering.

His research interests include wireless power transfer and matrix converter.

Mei Su was born in Hunan, China, in 1967. She received the B.S. degree in automation and the M.S. and Ph.D. degrees in electric engineering from Central South University, Changsha, China, in 1989, 1992, and 2005, respectively.

Since 2006, she has been a Professor with the School of Information Science and Engineering, Central South University. Her research interests include matrix converter, adjustable speed drives, and wind energy conversion system.

Yao Sun (M'13) was born in Hunan, China, in 1981. He received the B.S. degree in automation and M.S. and Ph.D. degrees in electric engineering from Central South University, Changsha, China, in 2004, 2007, and 2010, respectively.

He has been a Professor with the School of Information Science and Engineering, Central South University. His research interests include matrix converter, microgrid, and wind energy conversion system.

Weiyi Tang was born in Jiangsu, China, in 1991. He received the B.S. degree in automation from the Central South University, Changsha, China, in 2013, where he is currently working toward the Ph.D. degree in control science and engineering.

His research interests include motor control.

Aiguo Patrick Hu (SM'07) received the B.E. and M.E. degrees in electrical engineering from Xi'an JiaoTong University, Xi'an, China, in 1985 and 1988, respectively, and the Ph.D. degree in electrical and electronic engineering from the University of Auckland, Auckland, New Zealand, in 2001.

Before receiving the Ph.D. degree, he served as a Lecturer, the Director of China Italy Cooperative Technical Training Center, Xi'an, China, and the General Manager of a technical development company. Funded by Asian2000 Foundation, he stayed in the National University of Singapore for a semester as an Exchange Postdoctoral Research Fellow. He is a leading researcher in wireless power technologies. He is currently the Deputy Head (Research) of the Department of Electrical and Electronic Engineering, University of Auckland. He is also the Head of Research of PowerbyProxi Ltd, Auckland, New Zealand, as well as a Guest Professor of ChongQing Univ, Chongqing, China, and TaiYuan Univ of Technology, Taiyuan, China. He has been a foreign expert reviewer of 973 projects for the Chinese Ministry of Science and Technology, and an assessor of ChangJiang Scholars for the Ministry of Education. He is the former Chairman of IEEE NZ Power Systems/Power Electronics Chapter, and the Immediate Past Chairman of New Zealand North Section. He served as a Secretary/Treasurer of the New Zealand Chinese Scientists Association, and is currently the Vice President. He holds more than 50 patents in wireless/contactless power transfer and microcomputer control technologies across the world, authored or co-authored more than 200 peer-reviewed journal and conference papers with more than 3500 citations, authored the first monograph on wireless inductive power transfer technology, and contributed 4 book chapters on inductive power transfer modeling/control as well as electrical machines. His research interests include wireless/contactless power transfer systems, and application of power electronics in renewable energy systems.

Dr. Hu was the recipient of the University of Auckland VC's Funded Research and Commercialization Medal in 2017.